RSC Advances

ROYAL SOCIETY OF CHEMISTRY

www.rsc.org/advances

Journal Name

RSCPublishing

ARTICLE

Novel double-cathode configuration to improve cycling stability of lithium-sulfur battery

Cite this: DOI: 10.1039/x0xx00000x

Chao Wu, Lixua Yuan*, Zhen Li, Ziqi Yi, Yanrong Li, Rui Zeng, Wei Zhang, Yunhui Huang*

Received 00th January 2012,
Accepted 00th January 2012

DOI: 10.1039/x0xx00000x

www.rsc.org/

Unsatisfactory cycling lifespan is a key problem to hinder the practical application for next-generation lithium-sulfur battery. Here we report a facile method to improve the cycling stability through a novel double-cathode configuration. In addition to the traditional cathode based on sulfur composite confined in mesoporous CMK-3 (denoted as S/CMK-3), an addtional cathode based on sulfur composite confined in microporous carbon sphere (denoted as S/MiPCS) is set between the S/CMK-3 cathode and separator, which not only functions as a physical barrier to suppress polysulfides immigrating to lithium anode but also contributes to the overall capacity with a moderate sulfur loading. The double-cathode cell (denoted as DCC) demonstrates a greatly improved cycling stability. After 50 cycles with deep discharge to 1 V at 0.5 C, the DCC shows a capacity retention of 70% whereas the single S/CMK-3 cathode only keeps 28%. Even replacing S/CMK-3 by pure S, the double cathode containing S/MiPCS still exhibits a remarkable improved cyclability. This impressive enhancement mainly benefits from the stable property of MiPCS and its "blocking and reutilization effect". It can be visually confirmed that no polysulfides generated upon discharge process when sulfur is confined within microporous carbon.

Introduction

Lithium-sulfur battery (Li-S) are getting ever-increasing attention due to their high energy density[1-3] compared with traditional lithium-ion batteries based on insertion mechanism with capacity limited by transition metal oxides or phosphates.[4-6] The theoretical capacity of S is 1672 mAh g^{-1} according to the given full reduction of S into lithium sulfide ($S_8 + 16Li^+ + 16e^- \rightleftarrows 8Li_2S$) and the average potential is 2.15 V *vs*. Li/Li^+, demonstrating a theoretical energy density of 2500 Wh kg^{-1} or 2800 Wh L^{-1}.[7-9] In addition, sulfur is abundant, low cost and environmentally benign.[10, 11] Therefore, Li-S battery shows great potential as next-generation high-energy storage devices.

However, the practical application of Li-S battery is limited by several problems: (1) low utilization of active material and poor rate performance mainly caused by insulating nature of S and its final discharge products (Li_2S_2, Li_2S);[3, 12, 13] (2) the internal "shuttle effect" created by polysulfide intermediates (Li_2S_x, x = 4-8) dissolved in the ether-based electrolyte, which not only causes active material loss, but also remarkably reduces the coulombic efficiency;[13-15] (3) volume expansion as large as 80% due to the density difference between S (2.07 g cm^{-3}) and Li_2S (1.66 g cm^{-3}, leading to pulverization of cathode structure.[6, 16] As a consequence, Li-S battery suffer from limited cycling life, low coulombic efficiency and poor rate performance.[17, 18]

Many efforts have been devoted to addressing these problems. The most effective way is to couple sulfur with various porous carbon materials. By constraining the growth of sulfur nanofiller within the pores of conductive carbon framework, the conductivity of the sulfur electrode can be greatly enhanced, while the volume expansion and the dissolution loss of polysulfides can be also suppressed.[19] Up to now, many carbon materials with different porous structures have been investigated as sulfur supporters, such as ordered/disordered or mesoporous/microporous carbon,[20-22] hierarchical porous carbon,[23] hollow carbon spheres,[24] carbon nanofibers,[17, 25] carbon foams[26] and some combinations of the above structures.[27] Graphene/rGO composites were also investigated as S supporters due to their high electric conductivity and flexible structure to sustain volume change.[13,

State Key Laboratory of Material Processing and Die & Mould Technology, School of Materials Science and Engineering, Huazhong University of Science and Technology, Wuhan, Hubei 430074, China. Tel./fax: +86 2787558421. Email: huangyh@hust.edu.cn (Yunhui Huang), yuanlixia@hust.edu.cn (Lixia Yuan).

† Electronic Supplementary Information (ESI) available. See DOI: 10.1039/b000000x/

[28-30] Oxygen-containing functional groups on GO have been confirmed to have an advantage in anchoring polysulfides.[31, 32]

Mesoporous carbon is one of the most widely-used hosts for sulphur,[19, 20, 33] which can realize a high sulfur loading and a high sulfur utilization due to its robust porous structure and high conductivity. But unfortunately, cycling stability of the cathode based on sulfur composite confined in mesoporous carbon is always unsatisfied. The main reason is S nanofillers in mesopores can still be accessed by organic liquid electrolyte solvents so that the dissolution of the polysulfides cannot be suppressed effectively. Recently, Manthiram et al. proposed a new approach to improve the cycle performance of sulfur cathode by inserting a free-standing carbon interlayer between the sulfur cathode and separator. In this battery configuration, the carbon interlayer can work as a polysulfides barrier to restrain the diffusion of the dissolved polysulfides, therefore the active material can be confined within the cathode side, so that the cycling stability can be greatly improved.[34-38] Although the interlayer configuration is very simple and effective, the overall capacity of the battery is considerably reduced since the additional interlayer does not contribute to the overall capacity.

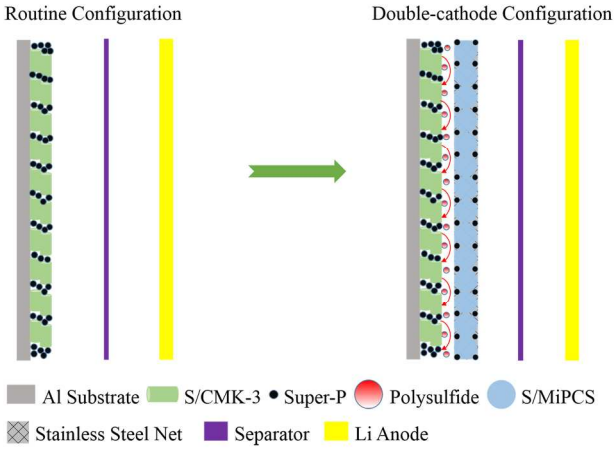

Fig. 1 Illustration of routine Li-S configuration and the present double-cathode configuration.

In this work, a novel double-cathode (DCC) is designed to improve the cycling stability of the sulfur cathode, as illustrated in Fig. 1. An additional cathode based on sulfur confined in microporous carbon was set between S/CMK-3 cathode and separator. It has been proved that sulfur confined in the microporous carbon exists as smaller sulfur molecule state (S_{2-4}) due to the space limit, thus no soluble high-order polysulfides form during charge-discharge process.[22, 39] As a consequence, cathode based on sulfur confined in microporous carbon always demonstrates excellent cycling stability. In this novel double-cathode configuration, S/MiPCS cathode not only functions as a physical barrier to trap polysulfides between the two cathodes to suppress polysulfides immigrating to lithium anode, but also can reuse the dissolved polysulfides and contribute to the overall capacity with a moderate sulfur loading. Compared with the pure carbon interlayer without sulfur, this configuration is beneficial to the overall energy density of the battery.

Experimental

Synthesis of microporous carbon sphere (MiPCS). MiPCS was prepared by using sucrose as carbon source via a facile hydrothermal treatment followed by carbonization and then activation with KOH.[21, 40] Briefly, 9 g sucrose (Sinopharm Chemical Reagent Co., Ltd.), 60 mg sodium dodecyl sulfate (SDS, Sinopharm Chemical Reagent Co., Ltd.) and 60 mL DI were mixed together. After sonication for 1 min, the mixture was sealed into a 100 mL Teflon autoclave for hydrothermal treatment at 180 °C for 4 h. The obtained dark brown precipitation was filtrated, washed, dried and calcined at 900 °C for 5 h in nitrogen atmosphere to get carbon sphere (CS). The CS and KOH were mixed in a ratio of 1:3 (w/w). Distilled (DI) water was added till all solid components were immersed. The suspension was stirred at 80 °C till a black slurry was formed. Then it was transferred to a homemade nickel box to be heated at 700 °C for 1 h in nitrogen atmosphere. MiPCS was collected by filtration, washed with 2 mol L^{-1} HCl and DI water till the filtrate became neutral.

Preparation of S/MiPCS and S/CMK-3 composites. The S/MiPCS composite was prepared through a simple heating method. Briefly, S and MiPCS were well mixed by grinding in a weight ratio of 3:7. The mixture was sealed in a stainless steel autoclave, and heated at 155 °C for 12 h and then at 300 °C for another 3 h. The S/CMK-3 composite was prepared via a route similar to S/MiPCS. Mesoporous carbon CMK-3 was purchased from Jiaxing Tanli New Materials R&D Co., Ltd. In a typical process, S and CMK-3 were well mixed by grinding with a weight ratio of 2:1, and then sealed in a Teflon autoclave followed by heating at 155 °C for 12 h. Sulfur loading in CMK-3 single-cathode and DCC is 1.35 mg cm^{-2} and 2.29 mg cm^{-2}, respectively.

Characterizations. Morphologies of MiPCS and CMK-3 were observed by scanning electron microscopy (SEM, FEI, SIRION200). Transmission electron microscopy (TEM) images were obtained by Tecnai G200 (FEI, Holland). X-ray diffraction (XRD) patterns were measured on an X-ray powder diffraction (PANalytical X'pert PRO-DY2198, Holland) operating at 40 kV and 40 mA using Cu Kα radiation (λ = 0.15406 nm). S content was determined by thermo-gravimetric analysis (TGA, PerkinElmer Instruments) in Ar at a heating rate of 10 °C min^{-1} from room temperature to 800 °C. Nitrogen adsorption/desorption isothermals of CMK-3 were measured with a Micrometritics ASAP 2020 analyzer (US) at -196 °C.

Electrochemical measurements. The S/CMK-3 cathode was fabricated in following procedure. S/CMK-3, super P, styrene butadiene rubber (SBR) (Sigma-Aldrich) and carboxyl methyl cellulose sodium (NaCMC) (Sigma-Aldrich) were mixed in a

weight ratio of 7:2:0.5:0.5 to form homogeneous slurry. The slurry was coated onto an aluminum foil, and then dried at 80 °C in an oven overnight. The cathode film was punched into round discs with diameter of 8 mm and roll pressed. The S/MiPCS cathode was prepared in a similar process except the slurry was pasted on a stainless steel net (600 mesh). The cathode film was punched into 10 mm diameter discs. The obtained S/MiPCS and S/CMK-3 cathode films were pressed together on a pressing machine to get the DCC cathode. The pure S cathode was prepared by mixing 60% S, 30% super P and 10% binder (1:1 SBR/NaCMC, w/w). The double pure S cathode was fabricated in exactly the same route except that the S/CMK-3 cathode was replaced by the pure S cathode. Celgard 2300 was used as separator and lithium metal as anode. Electrolyte was 1 mol L^{-1} LiTFSI in a mixture of 1, 3-dioxolane (DOL) and 1, 2-dimethoxymethane (DME) (v/v = 1:1) (Zhangjiagang Guotai-Huarong New Chem. Mater. Co., Ltd.) with 0.2 mol L^{-1} $LiNO_3$ (Sigma-Aldrich) as addictive. CR 2032 coin cells were assembled in argon-filled glove box with water and oxygen content ≤ 0.5 ppm. Cyclic voltammogram (CV) was tested at a scanning rate of 0.1 mV s^{-1} in the voltage range of 1.0–3.0 V (*vs*. Li^+/Li) on an electrochemical workstation (CHI614b, Shanghai Chenhua Instrument Co., Ltd.). Galvanostatic discharge/charge tests were carried out on battery measurement system (Land, China).

Results and discussion

The SEM image of CMK-3 and the TEM image of MiPCS are shown in Fig. 2 and Fig. S1. The meso- and micro-pores can be clearly identified in CMK-3 and MiPCS, respectively, which can be further confirmed by N_2 adsorption/desorption isothermals in Fig. 3. CMK-3 shows remarkable type IV isothermals (IUPAC classification) with a typical cylinder mesopores hysteresis loop (Fig. 3a).[41] The pore size of CMK-3 is identified to be 4.34 nm by BJH method (Fig. 3c). MiPCS shows type I isothermals of micropores (Fig. 3b) with an average pore size of about 0.54 nm (H-K method) (Fig. 3d). Brunauer-Emmett-Teller (BET) surface area and total pore volume for CMK-3 are 900 m^2 g^{-1} and 1.09 cm^3 g^{-1}, respectively; while for MiPCS are 1211.8 m^2 g^{-1} and 0.53 cm^3 g^{-1}. The pore volume determine the sulfur loading ability directly, so the S content in CMK-3 should be much higher than that in MiPCS. The XRD patterns in Fig. S2 show broad (002) and (100) peaks in both CMK-3 and MiPCS, indicative of amorphous nature for carbon. No crystalline peaks associated with S can be observed in S/CMK-3 and S/MiPCS, demonstrating that almost all S particles are well confined in the carbon pores with very few or even no residual S on the surface. Determined by TGA (Fig. S3), the S content is 66.6% in CMK-3 and 28.4% in MiPCS.

As illustrated in Fig. 1, the double-cathode is fabricated via covering S/CMK-3 cathode film by S/MiPCS so that the formed polysulfides can be well trapped between the two cathode films. Fig. 4 shows the SEM images of this novel double cathode. We can clearly distinguish S/CMK-3 (Fig. 4a) and S/MiPCS (Fig. 4b) since their morphologies are quite different. We can also see from the cross-section of the double cathodes (Fig. 4c) that S/MiPCS layer contacts with S/CMK-3 layer intimately, which can afford good restrict for polysulfides. The energy dispersive X-ray analysis (EDX) patterns (Fig. 4d) reveal that the S loadings are different for CMK-3 and MiPCS. The S content in CMK-3 is much higher than that in MiPCS, which agrees well with our initial design. Peak signals of Na and Al come from SBR-NaCMC binder and Al current collector.

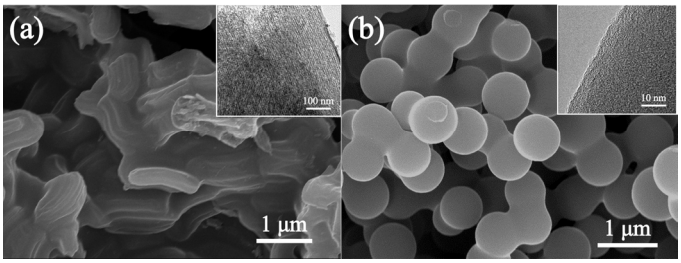

Fig. 2 SEM images of (a) CMK-3 and (b) MiPCS. The insets show their TEM images.

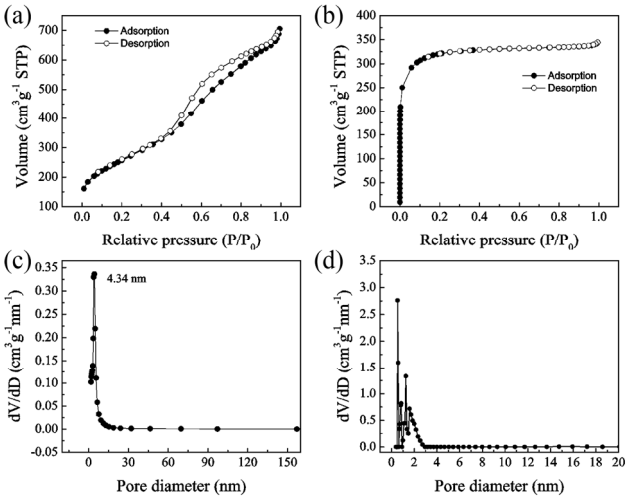

Fig. 3 Nitrogen adsorption/desorption isotherms of (a) CMK-3 and (c) MiPCS; pore size distribution of (b) CMK-3 and (d) MiPCS.

To evaluate the influence of the double-cathode configuration on electrochemical performance of S, the coin cells with the DCC film, individual S/CMK-3 and S/MiPCS as cathodes were tested under exactly the same condition. All cells are discharged to 1 V for the consideration of low voltage plateau of S/MiPCS. Since the activation phenomenon always appears in the first cycle, we choose the 2nd CV curves of the S/CMK-3, S/MiPCS and the DCC cathodes to reveal the stable redox behaviours of the electrode materials, as shown in Fig. 5a, 5b and 5c. Both of S/CMK-3 and S/MiPCS show their

typical electrochemical characteristics, which are similar with previous studies:[20, 22] S/CMK-3 shows two reductive peaks and one oxidative peak, while S/MiPCS shows a pair of wide redox peaks. As for the DCC electrode, it is interesting to find that there are three peaks at approximately 2.3, 2.0 and 1.5 V (*vs.* Li^+/Li) in the cathodic reduction process. The peaks at 2.3 and 2.0 V correspond to the reduction of S_8 molecule in the S/CMK-3 layer from S_8 to higher-order polysulfides (Li_2S_x, $4 < x < 8$), and then to lower-order lithium sulfides (such as Li_2S_2, Li_2S). The peak at 1.5 V is related to the reduction of smaller sulfur molecules in the S/MiPCS layer. In the subsequent anodic process, two oxidation peaks are observed at 2.1 and 2.6 V, which are attributed to the conversion of lithium sulfides to sulfur in micropores and mesopores, respectively. Obviously, the DCC electrode exhibits the combined redox features of both S/CMK-3 and S/MiPCS. In addition, the locations of redox peaks for DCC are almost identical with the S/CMK-3 cathode, indicating no kinetic barrier increased. The galvanostatic charge-discharge results agree well with CV testing. The DCC electrode shows three discharge plateaus, corresponding to the lithiation processes of the sulfur confined within mesopores (the S/CMK-3 layer) and the sulfur confined within micropores (the S/MiPCS layer), respectively (Fig. 5f). The reversible capacities of S/CMK-3, S/MiPCS and the DCC electrodes are 856, 957 and 915 mAh g^{-1}, respectively. Furthermore, it can be figured out that the capacity at above 1.8 V almost comes from S/CMK-3, while that below 1.8 V comes from both S/CMK-3 and S/MiPCS. Therefore, most capacity is ascribed to S/CMK-3, matching with the sulfur content in CMK-3 and MiPCS as well. The S content in CMK-3 is 2–3 times higher than that in MiPCS.

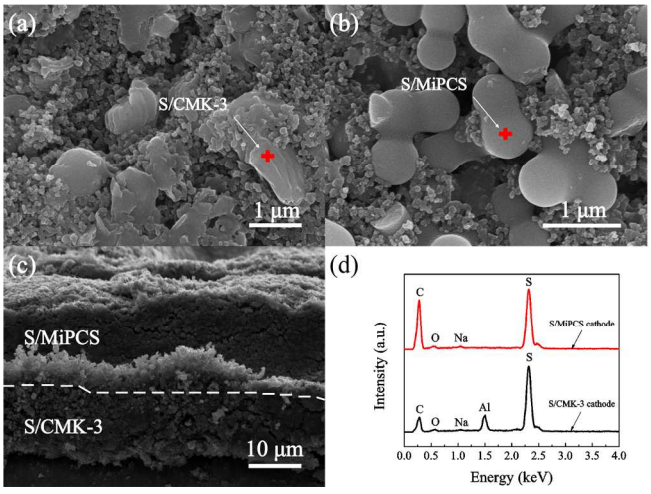

Fig. 4 SEM images of (a) S/CMK-3 cathode, (b) S/MiPCS cathode and (c) cross section of double cathodes. (d) EDX patterns of S/CMK-3 and S/MiPCS cathode.

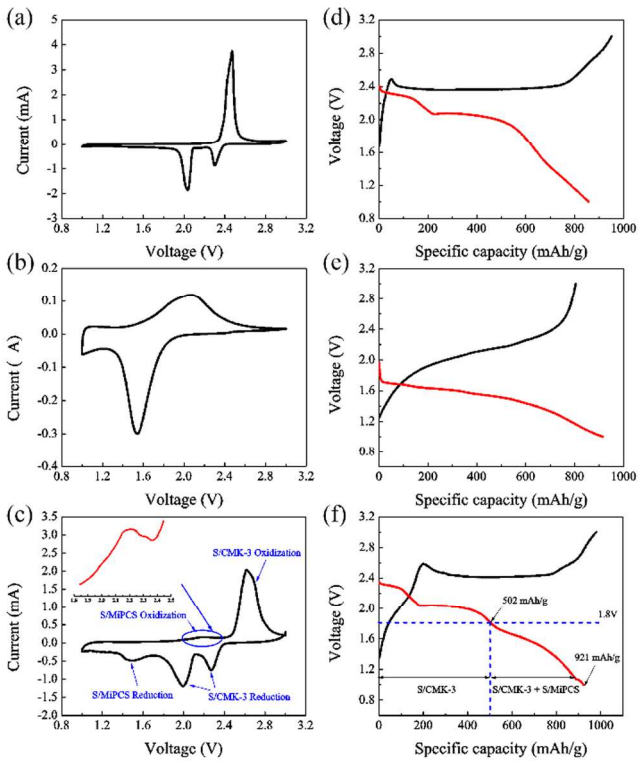

Fig. 5 Comparisons of the 2nd CVs (at a scanning rate of 0.1 mV s^{-1}) and charge-discharge profiles (at 0.5 C) in the 2nd cycle for (a, d) S/CMK-3, (b, e) S/MiPCS and (c, f) DCC.

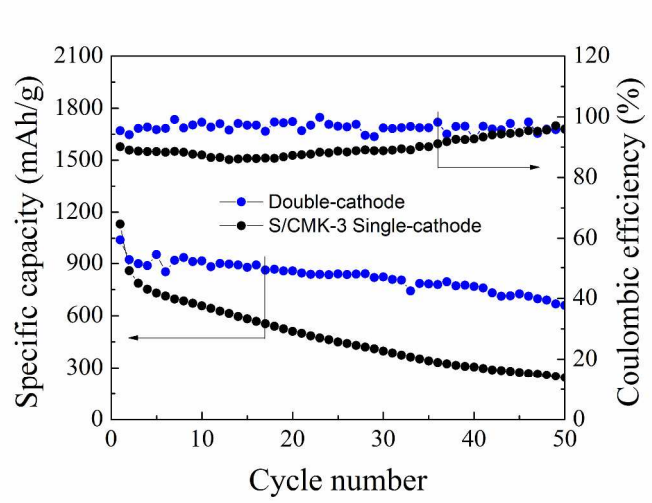

Fig. 6 Cycling performance and columbic efficiency for S/CMK-3 single-cathode and S/CMK-3@S/MiPCS double-cathode coin cells at 0.5 C.

Fig. S4 shows the cycling performance of the single S/MiPCS cathode, which exhibits an excellent cycling stability at 0.1C and 0.5C as previous studies.[21] Figure 6 compares the cycle performance between S/CMK-3 cathode and S/CMK-3@S/MiPCS (DCC) cathode. After the initial activation and

stabilization, the 2rd discharge capacities of S/CMK-3 and DCC are 856 and 915 mAh g^{-1}, respectively. The two cathodes show similar initial reversible capacity, but the DCC cathode demonstrate a much better cycling stability than that of the S/CMK-3 cathode. After 50 cycles, the capacity of DCC is still as high as 640 mAh g^{-1}, whereas S/MiPCS only retains 244 mAh g^{-1}. The corresponding capacity retentions are 70% and 28%, respectively. The great enhancement in capacity retention for DCC mainly results from its novel structure. The S/MiPCS interlayer cathode between S/CMK-3 cathode and separator can block and reuse the polysulfides generated from S/CMK-3, and hence improve the cycling performance. In addition, DCC shows an average coulombic efficiency of 97%, higher than 90% for S/CMK-3 cathode, which further confirms the DCC's blocking and reutilization effects. In order to demonstrate the advantage of DCC, a rough estimate of the gravimetric specific capacity and area specific capacity was made, as shown in Table S1. The DCC cathode demonstrates a specific gravimetric specific capacity which is a little lower than S/CMK-3 cathode, but much higher than S/MiPCS cathode. When considering the area specific capacity, the DCC shows more obvious advantage. The S/CMK-3 cathode gives an area specific capacity of 1.15 mAh cm^{-2}, while DCC demonstrates 1.34 mAh cm^{-2}. The above results indicate that the DCC cathode largely inherits the advantages of both mesoporous carbon (CMK-3) and microporous carbon (MiPCS).

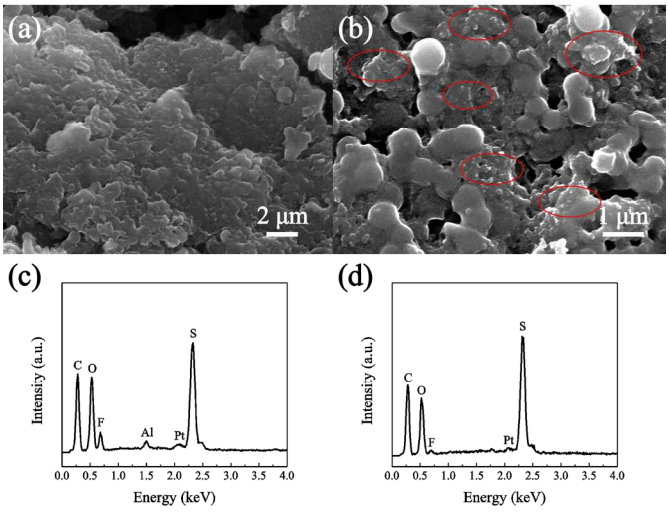

Fig. 7 Examination of a dissembled DCC coin cell after 50 cycles at 0.5 C: SEM images of (a) S/CMK-3 film and (b) S/MiPCS film; EDX spectra of (c) S/CMK-3 film and (b) S/MiPCS film.

The blocking and reutilization effects can be further proved by examining the dissembled cycled coin cell. Fig. 7 shows the SEM images of a dissembled DCC cell after running at 0.5 C for 50 cycles. The cycled S/CMK-3 cathode film shows an obviously changed morphology as compared to the fresh one. We can see a large number of solid agglomerates deposited on the electrode surface, which can be assigned to the irreversible Li_2S_2 and Li_2S particles.[42, 43] Some similar agglomerates can be also found on the corresponding interface of the S/MiPCS cathode film, as marked in red (Fig. 7b), demonstrating that the S/MiPCS interlayer can successfully prevent the poysulfides from diffusing to the anode side. The EDX measurements also support this result, as shown in Fig. 7c and 7d. After 50 cycles, the S content in S/CMK-3 greatly decreases, but the S content in S/MiPCS obviously increases. Apparently, the sulfur lost from the S/CMK-3 layer deposits on the S/MiPCS cathode, which can be reused in the subsequent cycles. Meanwhile, the morphology of S/MiPCS keeps well and no obvious evolution can be observed. As provided in Fig. S5b, the electrolyte collected from the cycled S/CMK-3 cathode has an obvious color change, which can be ascribed to the dissolution of the polysulfides. Interestingly, the electrolyte collected from the cycled S/MiPCS cathode keeps colorless and transparent even after 176 cycles (Fig. S5a), demonstrating that no polysulfides are formed in the S/MiPCS cathode over cycling (Fig. S5c). This indicates that the robust structure of S/MiPCS as the blocking layer.

In order to further validate the superiority of the double-cathode configuration, the coin cell with pure S@S/MiPCS double cathode was assembled. The fabrication process is exactly same as the S/CMK-3@S/MiPCS DCC cell except that the S/CMK-3 composite was replaced by pure sulfur. As shown in Fig. S6, the pure S@S/MiPCS double cathode exhibits a higher capacity over cycling compared with the pure S cathode. After 20 cycles, the S@S/MiPCS DCC cathode retains 74% capacity (*vs.* the 2rd cycle) while the pure S cathode only 38.1%. The DCC cathode realizes a much higher utilization of active material than the pure S cathode, implying that the S/MiPCS interlayer cathode can effectively reuse the dissolved polysulfides generated from the S cathode.

Conclusions

A simple and facile double-cathode configuration was proposed to improve the cycling stability of Li-S batteries. This novel cathode configuration largely inherits the advantages of both mesoporous carbon (CMK-3) and microporous carbon (MiPCS). The sulfur composite confined in mesoporous CMK-3 provides high capacity due to the high sulfur loading, while the sulfur composite confined in microporous carbon sphere acts as a physical barrier to prevent the formed polysulfides from immigrating to lithium anode and at the same time contributes to the overall capacity with a moderate sulfur loading. Such DCC cathode shows combined electrochemical performances of both S/CMK-3 and S/MiPCS. In particular, cycling stability is remarkably improved when compared with the single S/CMK-3 cathode. We believe that this novel configuration may find wide applications in high-performance Li-S batteries or other rechargeable batteries by exploring different inset cathodes with similar discharge/charge potential windows and further optimizing the DCC structure.

Acknowledgements

This work was supported by the National Science Foundation of China (Grant Nos. 21273087, 51002057 and 21271078), the 973 program (Grant No. 2015CB258400). The authors acknowledge the Analytical and Testing Center of HUST for XRD, FESEM, FETEM measurements, and the State Key Laboratory of Materials Processing and Die & Mould Technology of HUST for TG and BET.

Notes and references

1 P. G. Bruce, S. A. Freunberger, L. J. Hardwick and J. M. Tarascon, *Nat. Mater.*, 2012, **11**, 19.
2 Y. Yang, G. Y. Zheng and Y. Cui, *Chem. Soc. Rev.*, 2013, **42**, 3018.
3 C. Wang, W. Wan, J. T. Chen, H. H. Zhou, X. X. Zhang, L. X. Yuan and Y. H. Huang, *J. Mater. Chem. A*, 2013, **1**, 1716.
4 A. Manthiram, Y. Z. Fu and Y. S. Su, *ACCOUNTS OF CHEMICAL RESEARCH*, 2013, **46**, 1125.
5 B. C. Duan, W. K. Wang, A. B. Wang, Z. B. Yu, H. L. Zhao and Y. S. Yang, *J. Mater. Chem. A*, 2014, **2**, 308.
6 Y. Yang, G. H. Yu, J. J. Cha, H. Wu, M. Vosgueritchian, Y. Yao, Z. A. Bao and Y. Cui, *ACS NANO*, 2011, **5**, 9187.
7 X. L. Ji and L. F. Nazar, *J. Mater. Chem.* , 2010, **20**, 9821.
8 M. K. Song, E. J. Cairns and Y. G. Zhang, *Nanoscale*, 2013, **5**, 2186.
9 J. Hassoun and B. Scrosati, *Angew. Chem. Int. Ed.*, 2010, **49**, 2371.
10 S. Evers and L. F. Nazar, *ACCOUNTS OF CHEMICAL RESEARCH*, 2013, **46**, 1135.
11 R. Xu, I. Belharouak, J. C. M. Li, X. F. Zhang, I. Bloom and J. Bareño, *Adv. Energy Mater.*, 2013, **3**, 833.
12 Z. W. Zhang, Z. Q. Li, F. B. Hao, X. K. Wang, Q. Li, Y. X. Qi, R. H. Fan and L. W. Yin, *Adv. Funct. Mater.*, 2014, **24**, 2500.
13 B. Ding, C. Z. Yuan, L. F. Shen, G. Y. Xu, P. Nie, Q. X. Lai and X. G. Zhang, *J. Mater. Chem. A*, 2013, **1**, 1096.
14 S. Moon, Y. H. Jung, W. K. Jung, D. S. Jung, J. W. Choi and D. K. Kim, *Adv. Mater.*, 2013, **25**, 6547.
15 W. D. Zhou, Y. C. Yu, H. Chen, F. J. DiSalvo and H. D. Abruña, *J. Am. Chem. Soc.*, 2013, **135**, 16736.
16 W. Y. Li, G. Y. Zheng, Y. Yang, Z. W. Seh, N. Liu and Y. Cui, *PNAS*, 2013, **110**, 7148.
17 G. Y. Zheng, Q. F. Zhang, J. J. Cha, Y. Yang, W. Y. Li, Z. W. Seh and Y. Cui, *Nano lett.*, 2013, **13**, 1265.
18 W. Y. Li, Q. F. Zhang, G. Y. Zheng, Z. W. Seh, H. B. Yao and Y. Cui, *Nano lett.*, 2013, **13**, 5534.
19 F. G. Sun, J. T. Wang, H. C. Chen, W. M. Qiao, L. C. Ling and D. H. Long, *Sci. Rep.*, 2013, **3**, 2823.
20 X. L. Ji, K. T. Lee and L. F. Nazar, *Nat. Mater.*, 2009, **8**, 500.
21 H. Ye, Y. X. Yin, S. Xin and Y. G. Guo, *J. Mater. Chem. A*, 2013, **1**, 6602.
22 Z. Li, L. X. Yuan, Z. Q. Yi, Y. M. Sun, Y. Liu, Y. Jiang, Y. Shen, Y. Xin, Z. L. Zhang and Y. H. Huang, *Adv. Energy Mater.*, 2014, **4**, 1301473.
23 Y. H. Yin, C. Ma, Z. X. Cao, Z. X. Sun, Y. J. Jia and S. T. Yang, *RSC Adv.*, 2014, **4**, 28871.
24 C. F. Zhang, H. B. Wu, C. Z. Yuan, Z. P. Guo and X. W. Lou, *Angew. Chem. Int. Ed.*, 2012, **51**, 9592.
25 S. T. Lu, Y. Chen, X. H. Wu, Z. D. Wang, L. Y. Lv, W. Qin and L. X. Jiang, *Rsc Adv.*, 2014, **4**, 18052.
26 M. Depardieu, R. Janot, C. Sanchez, A. Bentaleb, C. Gervais, M. Birot, R. Demir-Cakan, R. Backov and M. Morcrette, *Rsc Adv.*, 2014, **4**, 23971.
27 D. W. Wang, G. M. Zhou, F. Li, K. H. Wu, G. Q. Lu, H. M. Cheng and I. R. Gentle, *Phys. Chem. Chem. Phys.*, 2012, **14**, 8703.
28 F. F. Zhang, X. B. Zhang, Y. H. Dong and L. M. Wang, *J. Mater. Chem.*, 2012, **22**, 11452.
29 H. Xu, Y. F. Deng, Z. C. Shi, Y. X. Qian, Y. Z. Meng and G. H. Chen, *J. Mater. Chem. A*, 2013, **1**, 15142.
30 J. Jin, Z. Y. Wen, G. Q. Ma, Y. Lu, Y. M. Cui, M. F. Wu, X. Liang and X. W. Wu, *RSC Adv.*, 2013, **3**, 2558.
31 L. W. Ji, M. M. Rao, H. M. Zheng, L. Zhang, Y. C. Li, W. H. Duan, J. H. Guo, E. J. Cairns and Y. G. Zhang, *J. Am. Chem. Soc.*, 2011, **133**, 18522.
32 J. P. Rong, M. Y. Ge, X. Fang and C. W. Zhou, *Nano lett.*, 2014, **14**, 473.
33 X. H. Zhao, D. S. Kim, J. Manuel, K. K. Cho, K. W. Kim, H. J. Ahn and J. H. Ahn, *J. Mater. Chem. A*, 2014, DOI: 10.1039/c4ta00490f.
34 Y. S. Su and A. Manthiram, *Nat. Commun.*, 2012, **3**, 1166.
35 Y. Z. Fu, Y. S. Su and A. Manthiram, *Adv. Energy Mater.*, 2014, **4**, 1300655.
36 S. H. Chung and A. Manthiram, *Chem. Commun.*, 2014, **50**, 4184.
37 Y. S. Su and A. Manthiram, *Chem. Commun.*, 2012, **48**, 8817.
38 S. H. Chung and A. Manthiram, *Adv. Mater.*, 2014, **26**, 1360.
39 S. Xin, L. Gu, N. H. Zhao, Y. X. Yin, L. J. Zhou, Y. G. Guo and L. J. Wan, *J. Am. Chem. Soc.*, 2012, **134**, 18510.
40 L. Qie, W. Chen, H. Xu, X. Xiong, Y. Jiang, F. Zou, X. Hu, Y. Xin, Z. Zhang and Y. Huang, *Energy Environ. Sci.*, 2013, **6**, 2497.
41 X. Y. Tao, X. R. Chen, Y. Xia, H. Huang, Y. P. Gan, R. Wu, F. Chen and W. K. Zhang, *J. Mater. Chem. A*, 2013, **1**, 3295.
42 Y. Diao, K. Xie, S. Z. Xiong and X. B. Hong, *J. Electrochem. Soc.*, 2012, **159**, A1816.
43 S. E. Cheon, K. S. Ko, J. H. Cho, S. W. Kim, E. Y. Chin and H. T. Kim, *J. Electrochem. Soc.*, 2003, **150**, A796.

